Geomechanics and Engineering, *Vol. 22, No. 4 (2020) 277-290*
DOI: https://doi.org/10.12989/gae.2020.22.4.277

Solution for surrounding rock of strain-softening considering confining pressure-dependent Young's modulus and nonlinear dilatancy

Peng Liang[1], Yongtao Gao[1], Yu Zhou[1], Chun Zhu*[2,3] and Yanhua Sun[4]

[1]Key Laboratory of Ministry of Education for Efficient Mining and Safety of Metal Mines, University of Science and Technology Beijing, Beijing 100083, China
[2]School of Earth Science and Engineering, Hohai University, Nanjing, 210098, China
[3]State Key Laboratory for Geomechanics and Deep Underground Engineering, Beijing 100083, China
[4]School of Civil Engineering, Guizhou University of Engineering Science, Bijie, 551700, China

(Received May 18, 2020, Revised July 1, 2020, Accepted July 8, 2020)

Abstract. This paper presents an elastic-plastic solution for the circular tunnel of elastic-strain softening behavior considering the pressure-dependent Young's modulus and the nonlinear dilatancy. The proposed solution is verified by the results of the field measuring and numerical simulation from a practical project, and a published closed-form analysis solution. The influence of each factor is discussed in detail, and the ability of Young's modulus and dilatancy characterizing the mechanical response of surrounding rock is investigated. It is found that, in low levels of support pressure, adopting the constant Young's modulus model will seriously misestimate the surrounding rock deformation. Using the constant dilatancy model will underestimate the surrounding rock deformation. When adopting the constant dilatancy model, as the dilation angle increases, the range of the plastic region increases, and the surrounding rock deformation weakens. When adopting the nonlinear dilatancy, the plastic region range and the surrounding rock deformation are the largest. The surrounding rock deformation using pressure-dependent Young's modulus model is between those resulted from two constant Young's modulus models. The constant α of pressure-dependent Young's modulus model is the main factor affecting the tunnel displacement. The influence of α using a constant dilatancy model is much more apparent than that using a nonlinear dilatancy model.

Keywords: circular tunnel; strain-softening behavior; Young's modulus; nonlinear dilatancy; generalized Hoek-Brown yield criterion

1. Introduction

The stability analysis of rock mass of underground engineering is of great significance in the development of mining engineering, petroleum engineering, civil engineering and hydraulic engineering. Many scholars have conducted numerous researches on rock stability by theoretical analysis (Shan and Lai, 2020), laboratory tests (Yin *et al*. 2017, Huang *et al*. 2020, Zhang *et al*. 2020a), numerical simulation (Wang *et al*. 2020a), similar model tests (Zhang *et al*. 2020b) and field tests (Tao *et al*. 2019, Wang *et al*. 2019, 2020b). The accurate evaluation of stress and deformation of rock mass around an excavation is one of the fundamental problems in underground engineering. It is of special importance for the stability evaluation and optimum structural design in tunnel engineering. Over the last few decades, numerous achievements have been made regarding the mechanical behavior of surrounding rock for circular openings by considering the elastic-perfectly plastic (EPP) model (Carranza-Torres and Fairhurst 1999), elastic-brittle plastic (EBP) model (Zhang *et al*. 2012a,b) and elastic-strain softening (ESS) model (Fahimifar *et al*. 2015, Cui *et al*. 2017, Cui *et al*. 2019, Zou *et al*. 2019).

∗Corresponding author, Lecturer
E-mail: zhuchuncumtb@163.com

The above mechanical models of rock masses behavior (i.e., EPP, EBP, ESS) can be defined based on the post-peak responses of the stress-strain curves in the failure process of rock masses. Hoek and Brown (1997) suggested that the EPP, ESS, and EBP models were available for the poor-quality, average-quality, and very high-quality rock masses, respectively. Furthermore, the EPP and EBP models refer to two extreme cases of the ESS model, and the ESS model can be considered as the most common case (Li *et al*. 2015). In other words, the ESS model covers every type of rock masses. Because of this observation, the main focus of the present study is the issues associated with the ESS model. Assuming that the elastic strain of rock masses and dilatation angle of the softening region were constant, a stepwise procedure for estimating the mechanical response around the circular opening in the Hoek-Brown (H-B) ESS rock masses was presented by Brown *et al*. (1983). At a later point in time, some improved methods were developed to determine the ESS solutions of circular tunnels. For instance, using the integration techniques for ESS behavior in rock masses, Alonso *et al*. (2003) calculated the ground reaction curves of a circular opening. Lee and Pietruszczak (2008) presented a simple and practical stepwise program for the calculation of stresses and strains around the circular openings in ESS rock masses. Park *et al*. (2008) extended the procedure of Brown *et al*. (1983) for the cases of circular openings excavated in ESS rock masses by using

http://www.techno-press.org/?journal=gae&subpage=7
ISSN: 2005-307X (Print), 2092-6219 (Online)

the variable dilation angle and elastic strain increments in the plastic zone. Moreover, based on the previous solutions for the ESS behavior of rock masses, several more accurate and simplified methods are also proposed (Cui *et al*. 2015).

However, a limitation of the above works is that the evolutions of rock masses parameters around a circular opening with confining pressure are not considered. The majority of the laboratory results indicate that the mechanical and physical properties of the rock masses mainly depend on the stress state (Zhang *et al*. 2018), i.e., show the pressure-dependent effect. For tunnels in rock masses, the in-situ stress redistribution due to the excavation will result in that Young's modulus and dilation angle are not constant (Yuan and Harrison 2004), but vary with the confining pressure within the plastic region. Considering the difference of Young's modulus between the plastic region and the elastic region, Sharan (2008) derived a closed-form solution for a circular opening excavated in H-B EBP rock masses. This solution depends on the assumption that Young's modulus within the plastic zone is smaller than that within the elastic region. For the rock masses around circular openings, Nawrocki and Dusseault (1995) presented two models to describe the nonlinear distribution of Young's modulus within the plastic region, namely the pressure-dependent modulus (PDM) model and the radius-dependent modulus (RDM) model. Brown *et al*. (1989) presented the solutions of circular openings in sandstone by considering the PDM model. Zhang *et al*. (2012a) proposed a closed-form solution to calculate the stresses and displacements of a circular opening within the UST (unified strength theory) EBP rock masses adopting the RDM model. Unfortunately, the above Young's modulus models are only adopted to the analysis of circular excavations in EBP rock masses, not for the ESS ones. Furthermore, regarding the dilatancy of rock masses, many existing analyses of the circular openings have always focused on the constant dilatancy rather than the variable one (Brown *et al*. 1983, Alonso *et al*. 2003, Park *et al*. 2008). Zhao and Cai (2010a) pointed out that a constant dilation angle was an approximation that was physically incorrect. For the issues of underground excavations, the dilation angle shows a decrease with the increase in confining pressure from the opening boundary to the deeper ground. Failure to account for the pressure-dependent dilatancy will result in calculation errors of the stability of underground openings. Detournay (1986) suggested the importance of the variable dilatancy and derived a plastic shear strain-dependent dilatancy model. Considering the effect of the stress state and plastic shear strain, several dilatancy models were established (Alejano and Alonso 2005, Zhao and Cai 2010a, b). Using the model of the nonconstant dilatancy proposed by Alejano and Alonso (2005) for the analysis of ground reaction curves of tunnels, Wang and Qian (2018) studied the stress and deformation of rock masses around circular openings. Although such variable dilatancy models have been considered to give insight into the elastic-plastic solutions of circular openings, it is unreasonable to neglect the influence of pressure-dependent Young's modulus in ESS rock masses.

Therefore, the main purpose of this paper is to propose a solution for the elastic-plastic analysis of the circular tunnel in ESS rock masses with comprehensive consideration given to the pressure-dependent Young's modulus and nonlinear dilatancy. Specifically, this study mainly includes four sections. The first section focuses on the problem definition by analyzing the ESS model corresponding to the H-B criterion, the pressure-dependent Young's modulus, and the nonlinear dilatancy. The second section then illustrates the procedure for the solution of the circular tunnels within H-B ESS rock masses. In the third section, the proposed solution is validated by adopting the field measurement data, numerical simulation results, and a published closed-form solution. Finally, the effects of both Young's modulus model parameters and dilatancy model parameters of ESS rock masses on the stress, plastic radius, and displacement are further investigated. The proposed solution and detailed research results could provide theoretical reference for the safety evaluation and optimal design of the tunnel support.

In contrast to the previous solutions, the proposed solution has the following innovations. The generalized Hoek-Brown yield criterion and the strain-softening model are considered for the rock mass. The influence of pressure-dependent Young's modulus on both stress and displacement is considered. The nonlinear dilatancy is considered by introducing the dilatancy angle related to confining pressure. The proposed solution can be applied to the practical projects.

2. Basic theory and problem definition

2.1 Mechanical model of a circular tunnel

The following basic assumptions are to be adopted in this analysis of the proposed solution:

(1) The cross-section of the tunnel is circular;

(2) The initial stress state of the tunnel is hydrostatic and constant with depth; and the stress distribution around the tunnel is axisymmetric;

(3) The rock is homogeneous, continuous, isotropic, and initially elastic; and it shows strain-softening behavior. The impact of the excavation disturbance is not considered;

(4) Plane strain conditions are assumed in the plane perpendicular to the tunnel axis; the circumferential and radial stress represent the major and the minor principal stress, respectively.

Based on the above assumptions, the mechanical model of a circular tunnel is illustrated in Fig. 1. p_0 represents the initial in-situ stress that exists before the tunnel. p_i is the internal support pressure, which uniformly distributes at the tunnel's surface. R_0 is the excavation radius of the circular tunnel. Under in-situ stress, the rock masses around a tunnel are composed of the plastic residual region and the plastic softening region. R_s and R_p are the radii of the residual region and the softening region, respectively. The circumferential and radial stresses of the elastic-plastic interface are represented by $\sigma_{\theta p}$ and σ_{rp}, respectively. Moreover, the circumferential and radial stresses of the softening-residual interface are represented by $\sigma_{\theta s}$ and σ_{rs}, respectively.

2.2 Generalized H-B elastic-strain softening model

The generalized Hoek-Brown (H-B) criterion is an

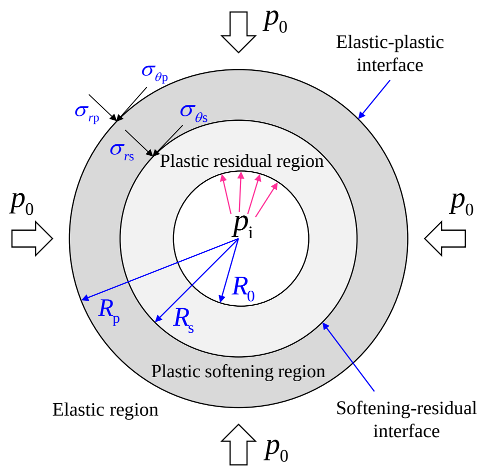

Fig. 1 Mechanical model of a circular tunnel

empirical criterion, and it can provide an estimation of rock mass strength. As a nonlinear criterion, it has been extensively applied in rock mass engineering, which is given as (Hoek *et al*. 2002):

$$\sigma_1=\sigma_3+\sigma_{ci}\left(m_b\sigma_3/\sigma_{ci}+s\right)^a \tag{1}$$

where σ_1 and σ_3 represent the major and minor principal stresses under triaxial compression conditions, respectively; σ_{ci} indicates the unconfined compressive strength for the intact rock; m_b, s, and a are the rock mass material constants that describe the strength characteristics of H-B rock masses. The empirical expressions of the constants m_b, s, and a in Eq. (1) are as follows:

$$m_b=m_i\exp\left[(GSI-100)/(28-14D)\right] \tag{2}$$

$$s=\exp\left[(GSI-100)/(9-3D)\right] \tag{3}$$

$$a=1/2+(1/6)\left[\exp(-GSI/15)-\exp(-20/3)\right] \tag{4}$$

where m_i is a constant of the intact rock that depends on the quality and type of a rock mass; D represents the disturbance factor of rock masses; GSI represents the geological strength index, which could be obtained according to the outcrops and structures of the rock masses.

Concerning the strain-softening behavior of geomaterials, the extensively used plastic shear strain γ^p is applied as the plastic softening index (Alejano and Alonso 2005). The development of the post-peak yield surface and strength parameters is governed by γ^p, and is given as:

$$\gamma^p=\varepsilon_\theta^p-\varepsilon_r^p \tag{5}$$

where ε_θ^p and ε_r^p denote the circumferential and radial plastic strain, respectively.

According to the plasticity theory, the deformation of geomaterials can be explained by the plastic potential g and the yield criterion f (Kaliszky 1989). For the strain-softening behavior of rock masses, g and f are both governed by the stress tensor σ_{ij} and the plastic softening index γ^p. Thus, the yield criterion f for ESS rock masses can be written as:

$$f(\sigma_{ij},\gamma^p)=0 \tag{6}$$

Using Eqs. (1) and (6), the H-B criterion for rock masses of the plastic softening region is then given by:

$$\begin{aligned}f(\sigma_\theta,\sigma_r,\gamma^p)&=\sigma_\theta-\sigma_r-\sigma_{ci}\left(m_b(\gamma^p)\sigma_r/\sigma_{ci}+s(\gamma^p)\right)^{a(\gamma^p)}\\&=0\end{aligned} \tag{7}$$

where σ_θ and σ_r represent the circumferential stress and radial stress, respectively; $m_b(\gamma^p)$, $s(\gamma^p)$ and $a(\gamma^p)$ represent the strength parameters of H-B ESS rock masses depending on γ^p. Generally, the evolution rule of the strength parameters is obtained by analyzing the results with the laboratory tests. For simplicity, a piecewise linear function is used to describe the relationship between γ^p and the strength parameters in this study, which can be defined in the following form:

$$\omega(\gamma^p)=\begin{cases}\omega^p-(\omega^p-\omega^r)(\gamma^p/\gamma^{p*}), & (0<\gamma^p<\gamma^{p*})\\ \omega^r, & (\gamma^p\ge\gamma^{p*})\end{cases} \tag{8}$$

where ω denotes a certain strength parameter of the H-B criterion, i.e., m_b, s and a; ω^r and ω^p stand for the residual and peak values of the m_b, s and a, respectively; and γ^{p*} is the critical value of the plastic softening index from softening to the residual stage of the surrounding rock. In the softening state, ω is set to reduce linearly with the increasing γ^p; while the ω remains invariable in the residual region. For the EPP behavior of rock masses, γ^p is considered to be a significantly large number (such as 100). Concerning the EBP behavior of rock masses, γ^p is 0.

2.3 Model of pressure-dependent Young's modulus

Numerous experimental investigations identify that Young's modulus is a significant parameter controlling the mechanical behavior of rock masses (Shi *et al*. 2018, Chen *et al*. 2019, Ren *et al*. 2019, Ren *et al*. 2020, Feng *et al*. 2020a, b). Hence, the Young's modulus model is of vital importance for successful evaluation of the stresses and strains around a tunnel. The Young's modulus of rock masses manifests a significant confining pressure effect, and it shows a nonlinear increase as the confining pressure increases. The decrease of Young's modulus is closely related to the gradual failure of the rock masses, which can explain the large deformation of surrounding rock observed from the tunnel's surface (Zhang *et al*. 2012a). Based on laboratory tests, some researchers (Kulhawy 1975, You 2003) concluded that an exponential equation could characterize the relationship between the confining pressure and Young's modulus. Furthermore, the conclusions by Brown *et al*. (1989) suggest that the evolution of Young's modulus could be considered as a nonlinear function of confining pressure, and the equation is expressed in the following form:

$$E(\sigma_r)=E_\infty-(E_\infty-E_0)\exp(-\alpha\times\sigma_r) \tag{9}$$

where E_0 denotes the Young's modulus value when the confining pressure is 0; E_∞ denotes the maximum Young's modulus at the critical stress state; α is a fitting constant that governs the non-linearity properties and varies for various rock masses.

For the rock masses around a circular tunnel, the E_0 in Eq. (9) denotes the Young's modulus on the tunnel's surface, and E_∞ denotes the Young's modulus at the elastic-plastic interface. In this study, the model proposed by Brown *et al*. (1989) is employed to calculate the stresses and displacements around the tunnels. According to whether Young's modulus varies with the confining pressure, two models are used in this paper, namely the constant Young's modulus model (referred to as CYM from hereon) and the pressure-dependent Young's modulus model (referred to as PYM from hereon).

2.4 Nonlinear dilatancy model

Experimental observations and engineering practices indicate that the rock dilatancy is directly linked to the failure process of a rock mass. In the elastic-plastic analysis of surrounding rock, dilatancy angle is widely used to measure the dilatancy capacity of rock masses. Therefore, the dilatancy angle is of considerable importance for calculating the stresses and displacements of tunnels. Essentially, an appropriate dilatancy model should be determined to better reflect the evolution of the rock failure mechanism, and to study the potential dilatancy process of the rock masses around a tunnel. Early studies of geotechnical engineering suggested that the dilation angle ψ was restricted to be equal to the friction angle φ in the associated flow rule. Subsequently, more recent studies noted that most geomaterials followed the non-associative flow rule, in which the ψ and the φ are unequal (Walton *et al*. 2019). Based on the engineering practices, Hoek and Brown (1997) suggested that the constant dilation angle ψ of $\psi = 0$, $\psi = \varphi^{\mathrm{p}} / 8$ and $\psi = \varphi^{\mathrm{p}} / 4$ for the poor-quality, average-quality and very high-quality rock masses, respectively. According to the experimental studies, however, some researchers asserted that the dilatancy was strongly influenced by the confining pressure (Yuan and Harrison 2004), and the dilation angle gradually decreased with the increase of confining pressure. Furthermore, some researchers presented various dilatancy models to integrate the effect of dilatancy on rock engineering (Alejano and Alonso 2005, Zhao and Cai 2010b).

For the H-B ESS rock masses, Alejano and Alonso (2005) pointed out that the peak value of the friction factor K_φ^{p} could be estimated by the envelope slope of the corresponding H-B criterion under a defined confining pressure, as follows:

$$K_\varphi^{\mathrm{p}} = \partial\sigma_1 / \partial\sigma_3 = 1 + a^{\mathrm{p}} m_b^{\mathrm{p}} \left(m_b^{\mathrm{p}} \sigma_3/\sigma_{\mathrm{ci}} + s^{\mathrm{p}} \right)^{a^{\mathrm{p}}-1} \tag{10}$$

$$K_\varphi^{\mathrm{p}} = (1+\sin\varphi^{\mathrm{p}}) / (1-\sin\varphi^{\mathrm{p}}) \tag{11}$$

where φ^p is the peak value of friction angle.

Combining Eqs. (10) and (11), the value φ^p is obtained, which is given by:

$$\varphi^{\mathrm{p}} = \arcsin \frac{a^{\mathrm{p}} m_b^{\mathrm{p}} \left(m_b^{\mathrm{p}} \sigma_3/\sigma_{\mathrm{ci}} + s^{\mathrm{p}} \right)^{a^{\mathrm{p}}-1}}{2 + a^{\mathrm{p}} m_b^{\mathrm{p}} \left(m_b^{\mathrm{p}} \sigma_3/\sigma_{\mathrm{ci}} + s^{\mathrm{p}} \right)^{a^{\mathrm{p}}-1}} \tag{12}$$

Besides, an empirical equation for the peak value of dilatancy angle ψ^p considering φ^p and confining pressure σ_3 was derived by Alejano and Alonso (2005), which has the following form:

$$\psi^{\mathrm{p}} = \frac{\varphi^{\mathrm{p}}}{1+\lg\sigma_{\mathrm{ci}}} \lg \frac{\sigma_{\mathrm{ci}}}{\sigma_3 + 0.1} \tag{13}$$

For circular tunnels, Detournay (1986) established the expression to describe the dilatancy factor, as flows:

$$\beta_\psi = 1 + (\beta_\psi^{\mathrm{p}} - 1)\exp\left(-\gamma^{\mathrm{p}}/\gamma^{\mathrm{p}*}\right) \tag{14}$$

where β_ψ is the dilatancy factor; β_ψ^{p} is the peak value of the dilatancy factor, and it can be obtained by $\beta_\psi^{\mathrm{p}} = (1+\sin\psi^{\mathrm{p}})/(1-\sin\psi^{\mathrm{p}})$.

By combining Eqs. (12), (13) and (14), the dilatancy factor β_ψ in H-B ESS rock masses can be obtained:

$$\left.\begin{aligned} &\beta_\psi = 1 + \left[(2\sin\psi^{\mathrm{p}})/(1-\sin\psi^{\mathrm{p}})\right]\exp\left(-\gamma^{\mathrm{p}}/\gamma^{\mathrm{p}*}\right) \\ &\psi^{\mathrm{p}} = \frac{\arcsin \dfrac{a^{\mathrm{p}} m_b^{\mathrm{p}} \left(m_b^{\mathrm{p}} \sigma_3/\sigma_{\mathrm{ci}} + s^{\mathrm{p}} \right)^{a^{\mathrm{p}}-1}}{2 + a^{\mathrm{p}} m_b^{\mathrm{p}} \left(m_b^{\mathrm{p}} \sigma_3/\sigma_{\mathrm{ci}} + s^{\mathrm{p}} \right)^{a^{\mathrm{p}}-1}}}{1+\lg\sigma_{\mathrm{ci}}} \lg \frac{\sigma_{\mathrm{ci}}}{\sigma_3 + 0.1} \end{aligned}\right\} \tag{15}$$

Eq. (15) presents the nonlinear dilatancy model (referred to as NDM from hereon) of H-B ESS rock masses around tunnels in the plastic region. This equation illustrates that the dilatancy factor β_ψ strongly depends on the confining pressure σ_3, the critical value of the plastic softening index γ^{p*}, and the plastic softening index γ^p. In the present study, the NDM and the CDM (constant dilatancy model) are used. The NDM is determined using Eq. (15), while the CDM is determined by $\psi = \varphi^{\mathrm{P}} / 4$ and $\psi = \varphi^{\mathrm{P}} / 8$.

3. Methodology and solutions

3.1 Stresses and displacements of the elastic region

In the elastic region ($r \geqslant R_{\mathrm{p}}$), the radial stress σ_r^e, the circumferential stress σ_θ^e, and the displacement u^{e} can be calculated based on the elastic solution (Park *et al*. 2008, Cui *et al*. 2015, Wang *et al*. 2018), which can be expressed in the following form:

$$\left.\begin{aligned} \sigma_r^{\mathrm{e}} &= p_0 - \left(p_0 - \sigma_{r\mathrm{p}}\right)\left(R_{\mathrm{p}}/r\right)^2 \\ \sigma_\theta^{\mathrm{e}} &= p_0 + \left(p_0 - \sigma_{r\mathrm{p}}\right)\left(R_{\mathrm{p}}/r\right)^2 \\ u^{\mathrm{e}} &= \frac{1+\nu}{E_{\mathrm{e}}}\left(p_0 - \sigma_{r\mathrm{p}}\right)\frac{R_{\mathrm{p}}^2}{r} \end{aligned}\right\} \tag{16}$$

in which E_e donates the Young's modulus of rock masses of the elastic region, and E_e is equal to E_∞; v is the Poisson's ratio of rock masses.

By solving Eq. (16) at the external boundary of the plastic region, we derive the following equation:

$$\sigma_{\theta p} - \sigma_{rp} = 2(p_0 - \sigma_{rp}) \tag{17}$$

Substituting Eq. (17) into Eq. (1), the equation for σ_{rp} at the external boundary of the plastic region is obtained as follows:

$$\sigma_{ci}\left(m_b^p \sigma_{rp}/\sigma_{ci} + s^p\right)^{a^p} - 2(p_0 - \sigma_{rp}) = 0 \tag{18}$$

When the constant a in Eq. (18) is equal to 0.5, Eq. (18) has an exact analytical solution; when a is not equal to 0.5, this equation can be solved using the Newton–Raphson approach (Cui *et al*. 2015).

3.2 Stresses and displacements solution of the plastic region

For the EPP and EBP behaviors, the closed-form solutions of circular tunnels can be obtained. When coming up against an issue of the tunnel with ESS behavior, the development of a closed-form solution could generally become intractable since the material parameters vary with the γ^p. Thus, a finite difference approach to solve this issue was firstly presented by Brown *et al*. (1983). As a numerical method, it has been extensively invoked to achieve requirements in the ESS problem. In this study, based on the approach presented by Wang and Qian (2018), the improved solution is derived for the circular tunnel in ESS rock masses. The schematic illustration of a circular tunnel is presented in Fig. 2. It illustrates that the potential plastic region around the tunnel is divided into n concentric annuli. $\sigma_{\theta(i)}$ and $\sigma_{r(i)}$ denote the circumferential and radial stresses at the internal boundary of the ith annulus, respectively. $\sigma_{\theta(i-1)}$ and $\sigma_{r(i-1)}$ represent the circumferential and radial stresses at the external boundary of the ith annulus, respectively. The subscript (i) denotes that the corresponding variable changes with the development of $\sigma_{r(i)}$ in the ith annulus. Furthermore, at the external boundary of the plastic region, the $r_{(0)}$ is equal to R_p; at the tunnel's surface, $r_{(n)}$ is equal to R_0.

In this study, the radial stress difference $\Delta\sigma_r$ between the external and internal boundaries of the ith annulus is fixed, which is given as follows:

$$\Delta\sigma_r = \left(\sigma_{r(n)} - \sigma_{r(0)}\right)/n = \left(p_i - \sigma_{rp}\right)/n \tag{19}$$

where $\sigma_{r(0)}$ and $\sigma_{r(n)}$ represent the radial stresses of the elastic-plastic interface and the tunnel's surface, respectively.

Then, according to the $\Delta\sigma_r$ obtained by Eq. (19), the radial stress and circumferential stress at the ith annulus can be calculated by:

$$\left.\begin{aligned}\sigma_{r(i)} &= \sigma_{r(i-1)} + \Delta\sigma_r \\ \sigma_{\theta(i)} &= \sigma_{r(i)} + \sigma_{ci}\left(m_{b(i-1)}\sigma_{r(i)}/\sigma_{ci} + s_{(i-1)}\right)^{a_{(i-1)}}\end{aligned}\right\} \tag{20}$$

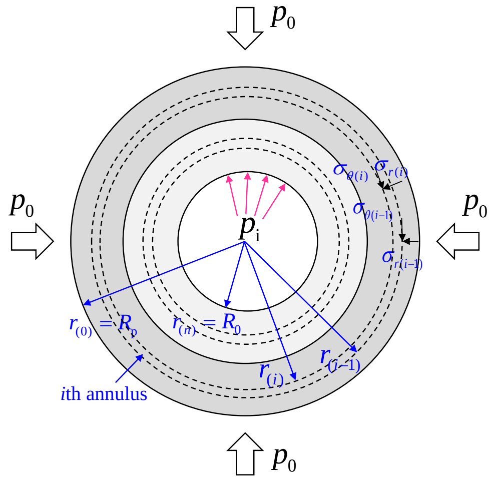

Fig. 2 The schematic diagram for layers in the plastic region

where $m_{b(i-1)}$, $s_{(i-1)}$, and $a_{(i-1)}$ are the strength parameters of the external boundary of the ith annulus, which can be calculated using Eq. (8). At the elastic-plastic interface (i = 0), $\gamma^p_{(0)}=0$, $m_{b(0)}=m_b^p$, $s_{(0)}=s^p$, $a_{(0)}=a^p$.

The stresses of the elastic-plastic interface (i = 0) is deduced as (Brown *et al*. 1983):

$$\begin{Bmatrix}\sigma_{r(0)} \\ \sigma_{\theta(0)}\end{Bmatrix} = \begin{Bmatrix}\sigma_{rp} \\ 2p_0 - \sigma_{rp}\end{Bmatrix} \tag{21}$$

where $\sigma_{r(0)}$ and $\sigma_{\theta(0)}$ are the radial and circumferential stresses at the elastic-plastic interface (i = 0).

The circumferential stress difference $\Delta\sigma_{\theta(i)}$ between the external and internal boundaries of the ith annulus is expressed in the following form:

$$\Delta\sigma_{\theta(i)} = \sigma_{\theta(i)} - \sigma_{\theta(i-1)} \tag{22}$$

For the ith annulus, in this study, the Young's modulus $\overline{E}_{(i)}$ is given as:

$$\overline{E}_{(i)} = (E_{(i)} + E_{(i-1)})/2 \tag{23}$$

where $E_{(i)}$ and $E_{(i-1)}$ represent the Young's moduli at the internal boundary and external boundary of the ith annulus, respectively, which can be given as follows:

$$\left.\begin{aligned}E_{(i)} &= E_\infty - (E_\infty - E_0)\exp\left(-\alpha\times\sigma_{r(i)}\right) \\ E_{(i-1)} &= E_\infty - (E_\infty - E_0)\exp\left(-\alpha\times\sigma_{r(i-1)}\right)\end{aligned}\right\} \tag{24}$$

Based on the generalized Hooke's law, the increments of elastic strain in the plane strain conditions are provided by:

$$\begin{Bmatrix}\Delta\varepsilon^e_{r(i)} \\ \Delta\varepsilon^e_{\theta(i)}\end{Bmatrix} = \frac{1+v}{\overline{E}_{(i)}}\begin{bmatrix}1-v & -v \\ -v & 1-v\end{bmatrix}\begin{Bmatrix}\Delta\sigma_{r(i)} \\ \Delta\sigma_{\theta(i)}\end{Bmatrix} \tag{25}$$

where $\Delta\varepsilon^e_{r(i)}$ and $\Delta\varepsilon^e_{\theta(i)}$ denote the radial and circumferential elastic strain increments of the ith annulus, respectively; v denotes the Poisson's ratio.

According to the results by Brown *et al*. (1983), the strains of the elastic-plastic interface (i = 0) are written as follows:

$$\begin{Bmatrix}\varepsilon_{r(0)}\\ \varepsilon_{\theta(0)}\end{Bmatrix}=\frac{1+\nu}{E_{\mathrm{e}}}\begin{Bmatrix}\sigma_{\mathrm{rp}}-p_0\\ p_0-\sigma_{\mathrm{rp}}\end{Bmatrix} \tag{26}$$

In the plane strain conditions, the strain increments include the plastic and elastic strain increments. Then, the following equation is derived:

$$\begin{Bmatrix}\varepsilon_{r(i)}\\ \varepsilon_{\theta(i)}\end{Bmatrix}=\begin{Bmatrix}\varepsilon_{r(i-1)}\\ \varepsilon_{\theta(i-1)}\end{Bmatrix}+\begin{Bmatrix}\Delta\varepsilon^{\mathrm{e}}_{r(i)}\\ \Delta\varepsilon^{\mathrm{e}}_{\theta(i)}\end{Bmatrix}+\begin{Bmatrix}\Delta\varepsilon^{\mathrm{p}}_{r(i)}\\ \Delta\varepsilon^{\mathrm{p}}_{\theta(i)}\end{Bmatrix} \tag{27}$$

where $\Delta\varepsilon^{\mathrm{p}}_{r(i)}$ and $\Delta\varepsilon^{\mathrm{p}}_{\theta(i)}$ denote the radial plastic strain increment and circumferential plastic strain increment, respectively.

Based on the non-associated flow rule, the relationship between the plastic strain increments and the dilatancy factor can be expressed as:

$$\Delta\varepsilon^{\mathrm{p}}_{r(i)}=-\beta_{\psi(i)}\Delta\varepsilon^{\mathrm{p}}_{\theta(i)} \tag{28}$$

where $\beta_{\psi(i)}$ represents the dilatancy factor at $r_{(i)}$ of the plastic region, which can be calculated from Eq. (15).

Substituting Eq. (28) into Eq. (27), the following equation can be obtained:

$$\begin{aligned}&\varepsilon_{r(i)}+\beta_{\psi(i)}\Delta\varepsilon_{\theta(i)}=\varepsilon_{r(i-1)}+\beta_{\psi(i)}\varepsilon_{\theta(i-1)}+\Delta\varepsilon^{\mathrm{e}}_{r(i)}+\beta_{\psi(i)}\Delta\varepsilon^{\mathrm{e}}_{\theta(i)}\\&+\Delta\varepsilon^{\mathrm{p}}_{r(i)}+\beta_{\psi(i)}\Delta\varepsilon^{\mathrm{p}}_{\theta(i)}=\varepsilon_{r(i-1)}+\beta_{\psi(i)}\Delta\varepsilon_{\theta(i-1)}+\Delta\varepsilon^{\mathrm{e}}_{r(i)}+\\&\beta_{\psi(i)}\Delta\varepsilon^{\mathrm{e}}_{\theta(i)}\end{aligned} \tag{29}$$

Setting

$B_{(i-1)}=\varepsilon_{r(i-1)}+\beta_{\psi(i)}\Delta\varepsilon_{\theta(i-1)}+\Delta\varepsilon^{\mathrm{e}}_{r(i)}+\beta_{\psi(i)}\Delta\varepsilon^{\mathrm{e}}_{\theta(i)}$ according to Wang and Qian (2018), $\varepsilon_{r(i)}$ and $\varepsilon_{\theta(i)}$ can be solved in the following form:

$$\left.\begin{aligned}\varepsilon_{r(i)}&=B_{(i-1)}-\beta_{\psi(i)}\Delta\varepsilon_{\theta(i)}\\ \varepsilon_{\theta(i)}&=\left(B_{(i-1)}-\varepsilon_{r(i)}\right)/\beta_{\psi(i)}\end{aligned}\right\} \tag{30}$$

In the plane strain conditions, the stress equilibrium equation irrespective of body forces can be written as follows (Timoshenko and Goodier 1982)

$$\frac{\partial\sigma_r}{\partial r}+\frac{\sigma_r-\sigma_\theta}{r}=0 \tag{31}$$

For the ith annulus, Eq. (31) can be approximated in the following form:

$$\frac{\sigma_{r(i)}-\sigma_{r(i-1)}}{r_{(i)}-r_{(i-1)}}-\frac{2H\left(\bar{\sigma}_{r(i)},\gamma^{\mathrm{p}}_{(i-1)}\right)}{r_{(i)}+r_{(i-1)}}=0 \tag{32}$$

in which $H\left(\bar{\sigma}_{r(i)},\gamma^{\mathrm{p}}_{(i-1)}\right)$ (referred to as H from hereon) is the function of H-B criterion parameters,

$H\left(\bar{\sigma}_{r(i)},\gamma^{\mathrm{p}}_{(i-1)}\right)=\sigma_{\mathrm{ci}}\left(m_{\mathrm{b}(i-1)}\bar{\sigma}_{r(i)}/\sigma_{\mathrm{ci}}+s_{(i-1)}\right)^{a_{(i-1)}}$ and $\bar{\sigma}_{r(i)}=\left(\sigma_{r(i)}+\sigma_{r(i-1)}\right)/2$

Then, the relationship between the $r_{(i)}$ and $r_{(i-1)}$ (referred to as $t_{(i)}$ from hereon) is deduced as:

$$t_{(i)}=\frac{r_{(i)}}{r_{(i-1)}}=\frac{2H+\Delta\sigma_r}{2H-\Delta\sigma_r} \tag{33}$$

The compatibility equation for strains is written as follows:

$$\frac{\partial\varepsilon_\theta}{\partial r}+\frac{\varepsilon_\theta-\varepsilon_r}{r}=0 \tag{34}$$

For the ith annulus, Eq. (34) can be approximated in an incremental form:

$$\frac{\varepsilon_{\theta(i)}-\varepsilon_{\theta(i-1)}}{r_{(i)}-r_{(i-1)}}+\frac{\varepsilon_{\theta(i)}+\varepsilon_{\theta(i-1)}-\varepsilon_{r(i)}-\varepsilon_{r(i-1)}}{r_{(i)}+r_{(i-1)}}=0 \tag{35}$$

Based on Eq. (35), the relationship between the $r_{(i)}$ and $r_{(i-1)}$ can also be written as:

$$\frac{r_{(i)}}{r_{(i-1)}}=\frac{2\varepsilon_{\theta(i-1)}-\varepsilon_{r(i)}-\varepsilon_{r(i-1)}}{2\varepsilon_{\theta(i)}-\varepsilon_{r(i)}-\varepsilon_{r(i-1)}}=t_{(i)} \tag{36}$$

By combining Eqs. (30)-(36), the radial strain and circumferential strain at $r_{(i)}$ can be derived in the following form:

$$\begin{cases}\varepsilon_{r(i)}=\dfrac{2t_{(i)}B_{(i-1)}/\beta_{\psi(i)}+\varepsilon_{r(i-1)}(1-t_{(i)})-2\varepsilon_{\theta(i-1)}}{2t_{(i)}/\beta_{\psi(i)}+t_{(i)}-1}\\[2ex] \varepsilon_{\theta(i)}=\dfrac{2\varepsilon_{\theta(i-1)}+(\varepsilon_{r(i-1)}+B_{(i-1)})(t_{(i)}-1)}{t_{(i)}(2+\beta_{\psi(i)})-\beta_{\psi(i)}}\end{cases} \tag{37}$$

where $t_{(i)}$ is the ratio of $r_{(i)}$ and $r_{(i-1)}$ that can be calculated using Eq. (33).

By rearranging Eq. (27), the plastic strain increments $\Delta\varepsilon^{\mathrm{p}}_{r(i)}$ and $\Delta\varepsilon^{\mathrm{p}}_{\theta(i)}$ of the plastic region are defined as:

$$\begin{Bmatrix}\Delta\varepsilon^{\mathrm{p}}_{r(i)}\\ \Delta\varepsilon^{\mathrm{p}}_{\theta(i)}\end{Bmatrix}=\begin{Bmatrix}\varepsilon_{r(i)}\\ \varepsilon_{\theta(i)}\end{Bmatrix}-\begin{Bmatrix}\varepsilon_{r(i-1)}\\ \varepsilon_{\theta(i-1)}\end{Bmatrix}-\begin{Bmatrix}\Delta\varepsilon^{\mathrm{e}}_{r(i)}\\ \Delta\varepsilon^{\mathrm{e}}_{\theta(i)}\end{Bmatrix} \tag{38}$$

According to Eq. (5), the plastic softening index γ^p of the ith annulus can be calculated as follows:

$$\gamma^{\mathrm{p}}_{(i)}=\gamma^{\mathrm{p}}_{(i-1)}+\Delta\gamma^{\mathrm{p}}_{(i)}=\gamma^{\mathrm{p}}_{(i-1)}+\left(\Delta\varepsilon^{\mathrm{p}}_{\theta(i)}-\Delta\varepsilon^{\mathrm{p}}_{r(i)}\right) \tag{39}$$

where $\Delta\varepsilon^{\mathrm{p}}_{\theta(i)}$ and $\Delta\varepsilon^{\mathrm{p}}_{r(i)}$ can be calculated by combining Eqs. (25), (37) and (38).

As described in section 2.2, $\gamma_{(i)}{}^p$ is in a state of change as σ_r develops from σ_{rp} to p_{i} in the plastic region. Hence, there is a position at fth annulus ($i = f$) where $\gamma_{(f)}{}^p$ approaches γ^{p*}. This position represents the transition from the softening region to the residual region. Thus, the radial stress $\sigma_{r(f)}$ is equal to σ_{rs} at this position.

The relation between the circumferential and radial strains with the displacement can be expressed as (Timoshenko and Goodier 1982):

$$\varepsilon_\theta=\frac{u}{r},\ \varepsilon_r=\frac{\partial u}{\partial r} \tag{40}$$

where ε_θ and ε_r are the circumferential and radial strains, respectively.

By combining Eqs. (1) and (31), the stress equilibrium equation of rock masses in the plastic residual region is derived as:

$$\frac{\partial \sigma_r}{\partial r}-\frac{\sigma_{\mathrm{ci}}\left(m_b^{\mathrm{r}}\sigma_r/\sigma_{\mathrm{ci}}+s^{\mathrm{r}}\right)^{a^{\mathrm{r}}}}{r}=0 \tag{41}$$

From Eq. (41), the radius of the residual region R_{s} is then obtained by the boundary conditions ($\sigma_r|_{r=R_0}=p_{\mathrm{i}}$ and $\sigma_r|_{r=R_{\mathrm{s}}}=\sigma_{r\mathrm{s}}$), giving:

$$R_{\mathrm{s}}=R_0\exp\left[\frac{\left(m_b^{\mathrm{r}}\sigma_{r\mathrm{s}}/\sigma_{\mathrm{ci}}+s^{\mathrm{r}}\right)^{1-a^{\mathrm{r}}}-\left(m_b^{\mathrm{r}}p_{\mathrm{i}}/\sigma_{\mathrm{ci}}+s^{\mathrm{r}}\right)^{1-a^{\mathrm{r}}}}{m_b^{\mathrm{r}}\left(1-a^{\mathrm{r}}\right)}\right] \tag{42}$$

Eq. (42) shows the relation between R_{s} and σ_{rs}. However, the value of R_{p} ($r_{(i)}$ at the elastic-plastic interface) is unknown. Therefore, multiplying Eq. (33), the relationship among R_0 and R_{p} for H-B ESS rock masses can be rewritten as follows:

$$\frac{r_{(n)}}{r_{(0)}}=\frac{R_0}{R_{\mathrm{p}}}=\prod_{i=0}^{i=n}\frac{2H+\Delta\sigma_r}{2H-\Delta\sigma_r} \tag{43}$$

The R_{p} can be calculated by Eq. (43). Therefore, the scope of the ith annulus $r_{(i)}$ can be deduced as:

$$r_{(i)}=R_{\mathrm{p}}\times\prod_{i=0}^{i}\frac{2H+\Delta\sigma_r}{2H-\Delta\sigma_r} \tag{44}$$

Combining Eqs. (37), (40) and (44), the radial displacement u at ith annulus is deduced as:

$$u_{(i)}=\varepsilon_{\theta(i)}r_{(i)}=\varepsilon_{\theta(i)}\times R_{\mathrm{p}}\times\prod_{i=0}^{i}\frac{2H+\Delta\sigma_r}{2H-\Delta\sigma_r} \tag{45}$$

Lee and Pietruszczak (2008) have analyzed the circular tunnel using another method. Although the proposed solution is similar to the work by Lee and Pietruszczak (2008), the procedure is totally different in the following aspects. Firstly, in Lee and Pietruszczak (2008), the influence of pressure-dependent Young's modulus and nonlinear dilatancy is not considered; secondly, the values of R_{s} and $\sigma_{r\mathrm{s}}$ are not solved in Lee and Pietruszczak (2008). In engineering applications, R_{s} and $\sigma_{r\mathrm{s}}$ are important parameters.

In the work of Lee and Pietruszczak (2008), it is pointed that the evolution of stress and displacement for n = 500 show good agreements with the exact solution. In addition, Wang *et al*. (2018) stated that as n increases from 500 to 2000, the values of R_{p} slightly increase, but its increase rate become small. Furthermore, after n reaches to 1500, the values R_{p} increase less and gradually converge. Therefore, in the present paper, n = 5000 is selected to ensure the sufficient accuracy. The flow chart for the proposed solution of the circular tunnel within H-B ESS rock masses is presented in Fig. 3. The corresponding procedure is presented in the following steps:

(1) Calculate σ_{rp} based on Eq. (18) and the radial stress increment $\Delta\sigma_r$ using Eq. (19).

(2) Calculate the radial stress $\sigma_{r(i)}$ and circumferential stress $\sigma_{\theta(i)}$ based on Eq. (20).

(3) Calculate the Young's modulus $\overline{E}_{(i)}$ using Eq. (23) and the dilatancy factor $\beta_{\psi(i)}$ by integrating $\sigma_{r(i)}$ into Eq. (15).

(4) Calculate $\Delta\varepsilon_{r(i)}^{\mathrm{e}}$ and $\Delta\varepsilon_{\theta(i)}^{\mathrm{e}}$ by integrating $\Delta\sigma_{r(i)}$, $\Delta\sigma_{\theta(i)}$ into Eq. (25). Solve $t_{(i)}$ using Eq. (36).

(5) Calculate the strain components $\varepsilon_{r(i)}$ and $\varepsilon_{\theta(i)}$ by integrating the values of $t_{(i)}$, $\beta_{\psi(i)}$ into Eq. (37).

(6) Calculate $\gamma_{(i)}^{\mathrm{p}}$ using Eq. (39), and judge whether or not $\gamma_{(i)}^{\mathrm{p}}=\gamma^{\mathrm{p}*}$. If yes, stop the calculation iteration and $\sigma_{r(i)}$ is equal to σ_{rs} at this position; the R_{s} can be solved using Eq. (42). Otherwise, set $i = i + 1$ and repeat steps (1)-(6).

(7) Calculate the softening region radius R_{p} and the radial displacement u using Eq. (43) and Eq. (45).

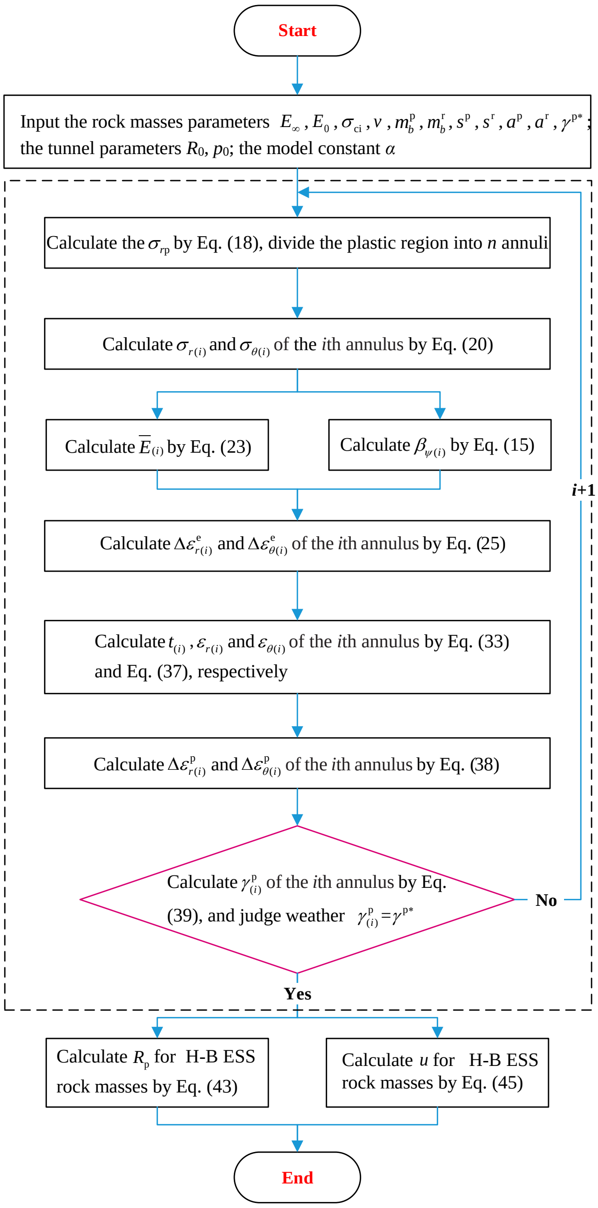

Fig. 3 Flow chart of the calculation procedure

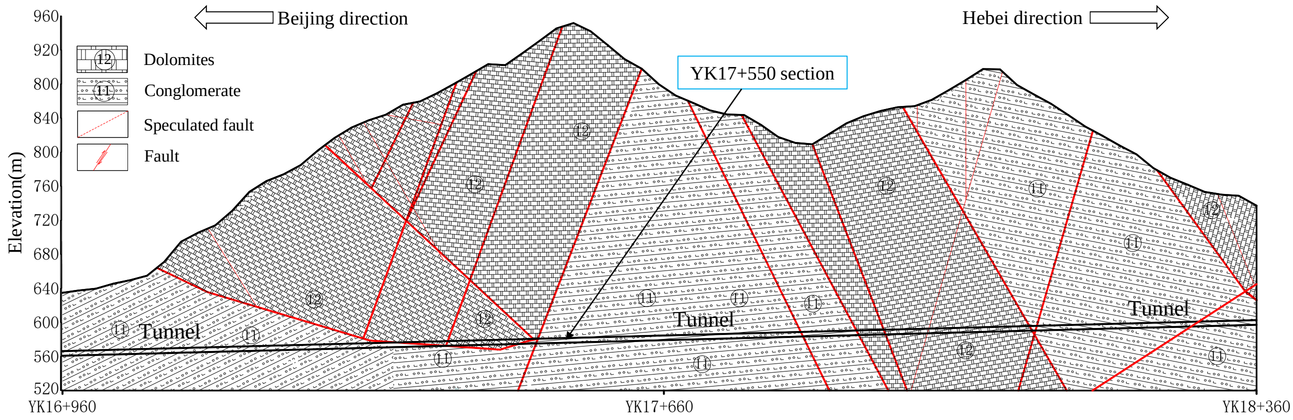

Fig. 4 Geological profile of the Yudushan tunnel

4. Example verifications

The proposed solution is validated by comparing with the field measurement results from a practical project named Yudushan tunnel and numerical results using the 3D finite-difference program FLAC3D. In addition, the proposed solution is compared and verified with a closed-form solution derived from the M-C criterion.

4.1 A comparison with the practical project

Yanchong expressway is a crucial project of a traffic guarantee system for the 2022 Beijing Winter Olympics, which has a total length of 114.4 kilometers. As an essential part of Yanchong expressway, the Yudushan tunnel with a bidirectional four lanes is located in Yanqing District, Beijing, China. The right line of the tunnel is from YK16+349 to YK 21+015, and the left line is from ZK16+363.3 to ZK20+955. The rock masses of the tunnel are dominated by dolomites, conglomerate, gneiss, and sandstone. Fig. 4 illustrates the engineering geological profile of the Yudushan tunnel from the Mileage of YK16+960 to YK18+360. The tunnel is excavated using the New Austrian Tunneling Method (NATM), and the tunnel in the study area is designed with a curved wall arch cross-section. The displacement, internal support pressure, and stress were measured on-site at several sections during the excavation process.

In this paper, the measuring data of the section YK17+550 are studied in detail. The test arrangements of the typical section are shown in Fig. 5. The section YK17+550 is located at an overburden depth of about 375 m. From the geological tests, the in-situ stress p_0 is 8.5 MPa. Based on the on-site geological survey and experimental test analysis, the physical and mechanical parameters of rock masses are as follows: R_0= 6.05 m, E_∞=11.4 GPa, E_0=5.2 GPa, σ_{ci}=46 MPa, v=0.26, α=0.043, m_b^p=3.0616, m_b^4=0.6091, s^{p}=0.0048, s^{r}=0.0000895, a^{p}=0.505, a^{r}=0.522, γ^{p*}=0.0085.

The formulations of the proposed solution are implemented using the fish code in every calculation step. For the Flac3D simulations, only a quarter of the geometry needs to be modeled due to the symmetry of the analyses problem (Jiang *et al*. 2020). The boundary is located at 30

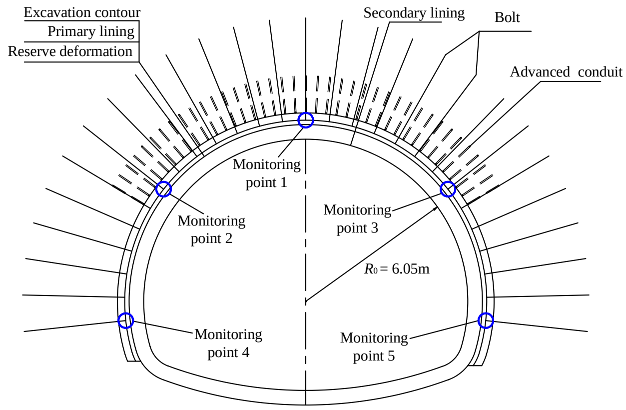

Fig. 5 Typical section details and the test arrangements of the Yudushan tunnel

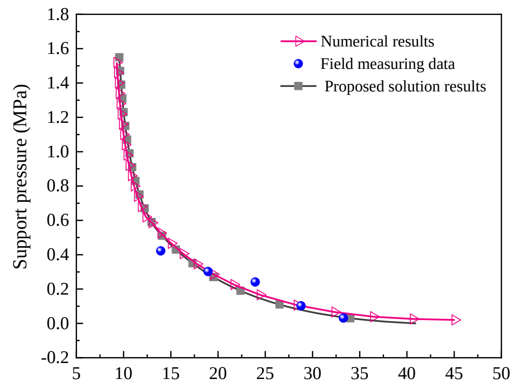

Fig. 6 Comparison of the proposed solution with the field measurement and FLAC3D

radii away from the center of the tunnel. The numerical model is composed of 8500 zones, as a plane strain model, the analysis plane is perpendicular to the axis of the tunnel. The normal velocities of grid points along the vertical, horizontal, bottom, front and back boundary planes are fixed at zero. The basic parameters of rock are the same as above. The proposed solution results are compared with the field measuring results and the numerical results, as illustrated in Fig. 6.

The results show that the proposed solution is consistent with the results of filed measurement and FLAC3D. As the support pressure decreases, the displacement gradually

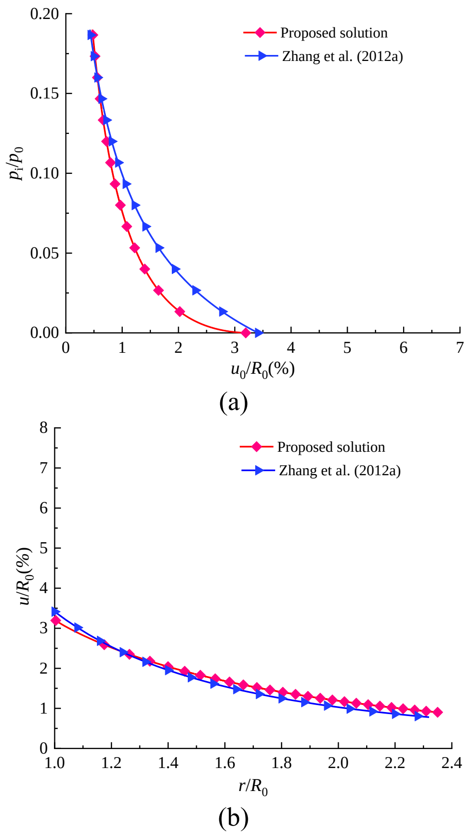

Fig. 7 Comparison results of the two solutions

increases. Meanwhile, the displacement reaches the maximum as the support pressure ultimately released. When the support pressure is completely discharged, the convergences of the tunnel's surface obtained by the proposed solution and FLAC3D are 40.96 mm and 45.07 mm, respectively. For defined support pressures, when the convergences calculated by the proposed solution are 15.46 mm 20.14 mm, the field measuring and numerical results are 13.94mm, 23.87mm, and 15.73 mm, 20.49 mm, respectively. The difference may be induced by that the proposed solution is based on numerous fundamental assumptions. Moreover, the field measurement is limited bythe geological conditions of the construction site and the measurement error, which is different from the real data.

4.2 A comparison with the closed-form solution

The comparison between the proposed solution and the solution derived by Zhang *et al.* (2012a) was carried out. As the EBP model is adopted in Zhang *et al.*'s analysis, the proposed solution using $\gamma^{p*}=0$ is adopted in this section. Moreover, as the H-B criterion is used in this paper without considering the intermediate principal stress, the solution using $b = 0$ by Zhang *et al.* is adopted (The solution using $b = 0$ of the unified strength theory degenerates to that of the M-C criterion). Furthermore, the influence of the nonlinear dilatancy is not considered in Zhang *et al.*'s analysis; thus, the CDM of $\psi = 0$ is used in this section. The other parameters are as follows: $R_0 = 2.5$ m, $p_0 = 150$ MPa, $\nu = 0.2$, $E_\infty = 42$ GPa, $E_0 = 10$ GPa, $\alpha = 0.05$, σ_{ci}=150 MPa, $m_b{}^p$=10.2, $m_b{}^p$=1.27, s^p=0.062, s^r=0.0002, a^p=0.5, a^r=0.51, γ^{p*}=0, c^p=14.1 MPa, c^r=6.4 MPa, φ^p=45.8°, φ^r=28.3°.

Fig. 7 shows the comparative results of the proposed solution and Zhang *et al.*'s solution. As illustrated in Fig. 7, the results obtained by the proposed solution are reasonably consistent with those calculated by the M-C criterion. It should be noted that there are certain differences in the values of convergence displacement for the defined support pressure between the two solutions in Fig. 7(a). When the support pressure is at a low level, the corresponding displacement calculated by Zhang *et al.*'s is larger. These differences are mainly due to the fact that the two solutions are derived from the H-B criterion and M-C criterion, respectively. Some researchers indicated that when the confining pressure around the rock is sufficiently small, the maximum allowable shear stress of rock with the H-B criterion is greater than that with the M-C criterion (Agar *et al.* 1987, Santarelli 1987). Furthermore, the stress obtained by the H-B criterion is more accurate (Hoek *et al.* 2002). Therefore, in the condition of low-level support pressure, the plastic region of the excavation with the H-B criterion is smaller than that with the M-C criterion. This means that a smaller displacement is obtained with the H-B criterion. Therefore, the results obtained in this paper are consistent with Zhang *et al.*'s results. Based on these reasons, the solution proposed in this study is reasonable and correct.

5. Parameter analysis

Some parametric analyses are conducted to study the far-reaching effect of the CYM, PYM, CDM, and NDM on the mechanical response of a circular tunnel. The parameters needed in this section are adopted as: tunnel radius $R_0 = 5$ m, in-situ stress $p_0 = 20$ MPa, uniaxial compressive strength σ_{ci}=80MPa, Poisson's ratio ν=0.25, $E_\infty = 9$ GPa, $E_0 = 5$ GPa, PYM constant $\alpha = 0.05$, $m_i = 12$. According to Sharan (2008), the peak disturbance factor D_p and the residual disturbance factor D_r are regarded as 0 and 0.5, respectively, to characterize the excavation disturbance. Furthermore, the peak value of the geological strength index is regarded as $GSI_p = 50$. The residual value of geological strength index GSI_r is calculated using the model presented by Alejano *et al.* (2012), which can be expressed as

$$GSI_r = 17.25\exp\left(0.0107 GSI_p\right) \tag{46}$$

By solving Eqs. (2)~(4) and Eq. (46), the parameters of rock materials are obtained, as shown in Table 1. In the CDM, two kinds of dilatation angle ($\psi = \varphi^p/4$ and $\psi = \varphi^p/8$) are used.

Table 1 Parameters of rock materials

Parameters	m_b	s	a	ν
Peak value	2.0121	0.0039	0.5057	0.25
Residual value	0.4171	0.00008	0.5232	0.25

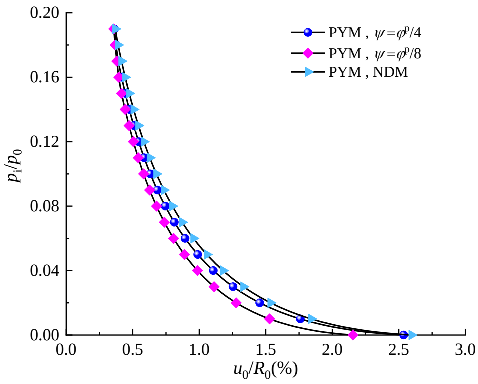

(a) Case A_1

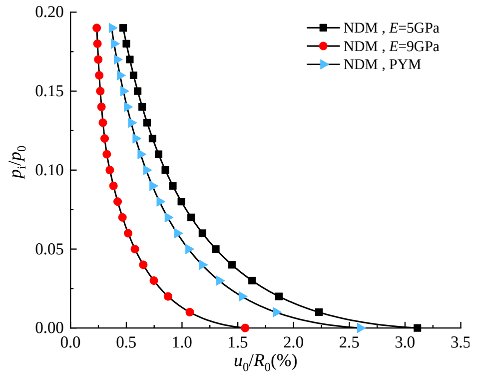

(b) Case A_2

Fig. 8 Influences of various models on ground reaction curves

5.1 Analysis of ground reaction curve

The convergence-confinement method is a standard and extensively used approach for support structure design in tunnel engineering. This method includes three different curves, i.e., the ground reaction curve (GRC), the longitudinal displacement profile (LDP), and the support characteristic curve (SCC) (Carranza-Torres and Fairhurst 2000). The GRC is developed with the application of flexible supports and the development of the New Austrian Tunneling Method. It applies the elastoplastic theory and rock mechanics to underground engineering to analyze the interaction process of surrounding rock and support. Moreover, it is a practical curve for the tunnel structure analysis combining theoretical basis, measured data, and engineering experience. In the convergence-confinement method, it can relate the internal pressure to the displacement of the tunnel's surface. In this paper, the GRC is selected to analyze the influences of Young's modulus and dilatancy on the mechanical response of a circular tunnel. Two examples that cases A_1 and A_2 are selected corresponding to the conditions of PYM and NDM described in section 2. For the results, case A_1 is assigned two kinds of dilatancy models, which are NDM and CDM ($\psi = \varphi^P / 4$ and $\psi = \varphi^P / 8$), respectively. Meanwhile, case A_2 is assigned two kinds of Young's modulus models, which are PYM and CYM (E = 5 GPa and E = 9 GPa), respectively.

Fig. 8(a) and 8(b) show the evolutions of GRCs under various Young's modulus models and dilatancy models for H-B ESS rock masses. Obviously, similar developments of GRCs for multiple conditions can be observed. In the case of A_1, the highest u_0 is obtained with the NDM at a defined support pressure. Furthermore, the lowest u_0 is achieved with the CDM ($\psi = \varphi^P / 8$) for a defined support pressure. The displacement u_0 may be underestimated when using a CDM, and the smaller the dilatation angle, the more significant the underestimation.

In the case of A_2, employing the two CYM of E = 5 GPa and E = 9 GPa results in the highest and the lowest u_0 for a defined support pressure, respectively. When the PYM is used, the resulting GRC is at an intermediate level. When the support pressure is at low levels, the displacement u_0 in the CYM conditions may be seriously overestimated or underestimated, which makes the engineering design relatively dangerous. For high levels of support pressure, the use of the CYM and PYM results in almost the same displacement u_0. The higher the support pressure, the smaller the plastic region and deformation of rock masses. Therefore, the effects of Young's modulus and dilatancy on the stresses and deformations of rock masses are weakened.

5.2 Analysis of plastic region range

To illustrate the influences of Young's modulus and dilatancy on the plastic region range, the CYM, PYM, CDM, and NDM are used to calculate the plastic region radius R_p and the plastic residual region radius R_s. Fig. 9 shows the evolutions of R_p and R_s concerning various models.

As the results plotted in Fig. 9 show, the extent of the R_p and R_s are clearly affected by the dilatancy and Young's modulus models. For a defined Young's modulus model, an increasing dilatation angle ψ in the CDM conditions increases the R_p and R_s, and the largest R_p and R_s can be obtained in the NDM condition. In the CYM condition, with an increase of Young's modulus (referred to as E from hereon), R_p and R_s decrease. Taking the case of $\psi = \varphi^P / 8$ as an example, when E increases from 5 GPa to 7 GPa, R_p and R_s decrease from 10.992 m, 10.064 m to 10.266 m, 8.548 m, with decreasing rates of 6.60% and 15.06%, and the decreasing rates of 6.23% and 13.54% correspond to the E increasing from 7 GPa to 9 GPa. Furthermore, for the case of $\psi = \varphi^P / 4$, R_p and R_s decrease from 11.147 m and 10.422 m to 10.471 m and 8.967 m when E increases from 5 GPa to 7 GPa, with decreasing rates of 6.06% and 13.96%, and the decreasing rates of 5.67% and 12.48% correspond to the E increasing from 7 GPa to 9 GPa. In the NDM condition, when the E increases from 5 GPa to 7 GPa, R_p and R_s decrease from 11.276 m and 10.674 m to 10.686 m and 9.377 m, with decreasing rates of 5.23% and 12.15%, and the decreasing rates of 4.61% and 10.16% correspond to the E increasing from 7 GPa to 9 GPa. It implies that when the Young's modulus model is CYM, the change of Rs is much more apparent than that of R_p with the increase of E. In other words, Young's modulus only influences the R_p slightly in the CYM conditions. In the CDM conditions, the Young's modulus model has a greater influence on R_p and R_s for a smaller dilatation angle ψ. Meanwhile, when the

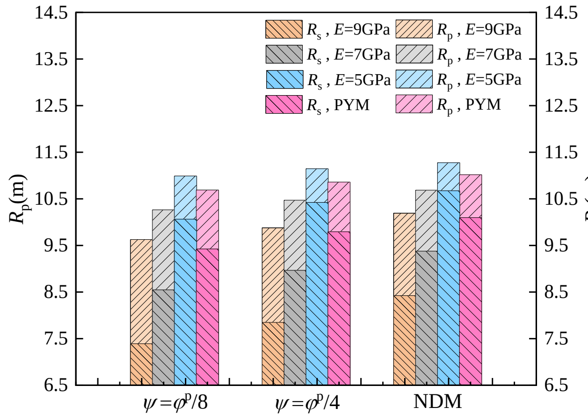

Fig. 9 Comparison of the R_p and R_s with different models

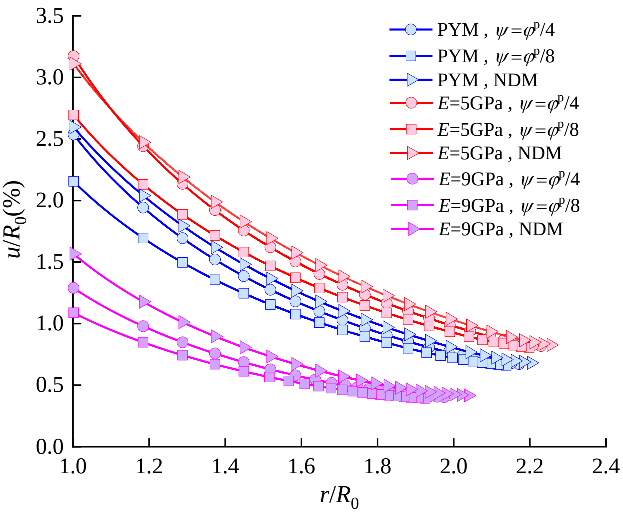

Fig. 10 Displacements of surrounding rock masses versus radius

Table 2 Statistics of the cases for multiple models

Models	Cases								
	B_1	B_2	B_3	B_4	B_5	B_6	B_7	B_8	B_9
E	PYM	PYM	PYM	5 GPa	5 GPa	5 GPa	9 GPa	9 GPa	9 GPa
ψ	NDM	φ^p / 4	φ^p / 8	NDM	φ^p / 4	φ^p / 8	NDM	φ^p / 4	φ^p / 8

dilatancy model is NDM, Young's modulus model has the least influence on R_p and R_s.

5.3 Analysis of plastic region displacement

This section chooses nine kinds of cases according to the various datasets to incorporate the overall influence of Young's modulus and dilatancy. Table 2 lists the statistical parameters varied in this section. Fig. 10 plots the evolution of the radial displacements u for various cases according to the input parameters listed in Table 2.

As observed from Fig. 10, the radial displacement u gradually decreases with the increasing radius r for all cases. Additionally, u is significantly influenced by the consideration of the Young's modulus and dilatancy models. It is interesting to see that this influence is much more pronounced at the position close to the tunnel's surface. Meanwhile, it can be concluded that for a defined dilatancy model, in general, u in the case of PYM (i.e., cases B_1, B_2, and B_3) are between the those of CYM (i.e., cases B_4, B_5, B_6, B_7, B_8, and B_9). Furthermore, it is worth noted that the minimum displacement is obtained in case B_9. Generally, for a defined Young's modulus model, the radial displacements in the case of NDM is reasonably larger than those in the case of CDM. For instance, the displacement of the tunnel's face increases by 20.46% as the condition varies from case B_3 to case B_1. Similarly, when the situations change from cases B_6, B_9 to cases B_4, B_7, the displacements of tunnel's surface increases by 15.43%, 43.88%, respectively. Therefore, neglecting the NDM will lead to the underestimation of tunnel radial displacement, which is also consistent with the analysis results in section 5.1. In view of this, we recommend to use the NDM as the dilatancy model for future elastic-plastic analysis and the design of tunnels. Moreover, Fig. 10 also suggests that for the same Young's modulus model, the displacements obtained by the CDM are very similar to those obtained by the NDM at the position near the elastic-plastic interface. It implies that the dilatancy model exerts a more significant effect on the zone near the tunnel's surface than that near the elastic-plastic interface.

5.4 Analysis of tunnel's surface displacement

In this section, three cases of Young's modulus conditions are defined for each dilatancy model, as listed in Table 3. Case C_1 does not consider the discrepancy of the E value between the elastic and plastic regions. Namely, case C_1 assumes a CYM model, in which the value of E is set from 5 GPa to 9 GPa at an interval of 0.5 GPa. Case C_2 is a PYM model given by Eq. (9), in which the value of E_0 is 5 GPa, and the value of E_∞ is set from 5 GPa to 9 GPa at an interval of 0.5 GPa. Case C_3 is also a PYM model; however, the value of E_∞ is 5 GPa, and the value of E_0 is set from 5 GPa to 9 GPa at an interval of 0.5 GPa. Meanwhile, the other parameters are all the same with the standard case. Then, the results of the tunnel's surface displacement u_0 obtained from case C_1, case C_2, and case C_3 are compared in Fig 11.

It can be found that the highest value of u_0 is obtained in the case of C_2 for a defined dilatancy model. Meanwhile, case C_3 generates the lowest value of u_0 in comparison to other cases. Thus, both cases C_2 and C_3 do consider the variability of the E value with radial stress in the plastic region and stand for two extreme estimations. The results of case C_1 are between those of case C_2 and case C_3. On the

Table 3 Distribution of Young's modulus conditions with the same dilatancy

Young's modulus condition		E / GPa	E_∞ / GPa	E_0 / GPa
Cases	Properties			
Case C_1	constant	5~9	—	—
Case C_2	variable	—	5~9	5
Case C_3	variable	—	9	5~9

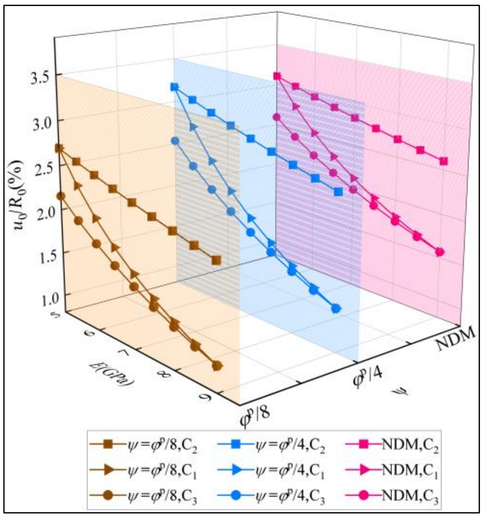

Fig. 11 Displacements of tunnel's surface with various modes

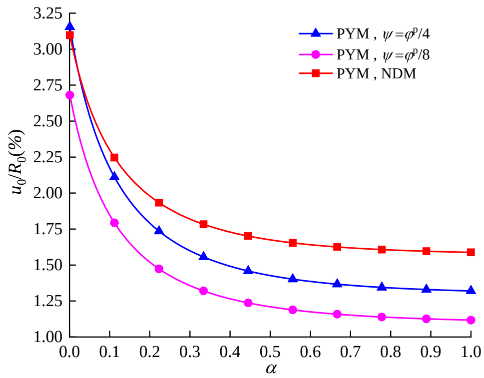

Fig. 12 The relation between the tunnel's surface displacement and PYM model constants

other hand, with the increase of the values of E, E_∞, and E_0 in rock masses, values of the tunnel's surface displacement u_0 all decrease. In particular, a sharp decrease of u_0 with the increasing E for case C$_1$ can be observed. The results show that the difference between E_∞ and E_0 is a key factor affecting the error between the CYM and PYM conditions. As such, a suitable choice of Young's modulus model has a significant effect on the tunnel design.

5.5 Influence of the PYM constant

To further study the influence of the PYM on the deformation of a circular tunnel, the evolution of the tunnel's surface displacement u_0 with the constant α is presented in Fig. 12, for three different dilatancy conditions. As can be seen from Fig. 12, the curves are very similar for all cases, namely, with the increasing α, u_0 decreases monotonically. It implies that the constant α on u_0 exhibits no evident dependence on the dilatancy model.

When the constant α is kept in a low-value range, the curves change considerably; namely, the u_0 changes significantly with α. When the α is in a high-value range, the curves change tends to be gentle, and the u_0 is basically not affected by the constant α. In the NDM condition, the u_0 decreases by 48.72% as the α increases from 0.001 to 1. Furthermore, using the two CDM ($\psi = \varphi^P / 4$, $\psi = \varphi^P / 8$) will cause the u_0 to be decreased by 58.31% and 58.16%, respectively, as the constant α increases from 0.001 to 1. Therefore, in the CDM, the constant α has a more significant effect on u_0; in the NDM, the u_0 is relatively less influenced by the α. Generally, for a defined constant α, the value of u_0 corresponding to NDM is the largest; the value of u_0 corresponding to CDM is relatively lower, and the smaller the dilation angle, the smaller the u_0. Furthermore, it can be seen that using the CDM condition will underestimate the deformation of the surrounding rock. Therefore, in practical engineering, reasonable use of Young's modulus, dilatancy is essential for the correct estimation of tunnel stability.

6. Conclusions

This paper has proposed a solution for the elastic-plastic analysis on the circular tunnel within H-B ESS rock masses considering nonlinear dilatancy and pressure-dependent Young's modulus. The main conclusions are summarized as follows:

- The highest tunnel deformation is obtained using the NDM for a defined support pressure. At low support pressure, the CYM will result in a misestimation of tunnel deformation. Meanwhile, the use of the CYM and PYM results in almost the same displacements at high support pressure.
- For a defined dilatancy model, the larger the value of E in the CYM, the smaller the R_p and R_s. For a defined Young's modulus model, the R_p and R_s in the CDM increase as the dilatancy angle ψ increases; the R_p and R_s in the NDM are the largest. In the NDM, R_p and R_s are least influenced by Young's modulus model.
- For a defined dilatancy model, the tunnel deformation corresponding to the PYM is between those obtained in the CYM. For a defined Young's modulus model, the tunnel deformation in the NDM is the largest. For a defined dilatancy model, the rise of E_∞ or E_0 in the PYM can both cause the tunnel's surface displacement u_0 to decrease.
- In the PYM, the u_0 decreases as the constant α increases. When α is in a low-value range, u_0 decreases rapidly; when α is in a high-value range, u_0 decreases slowly. In the NDM, u_0 is least influenced by α, and using the CDM will underestimate the tunnel deformation.

Acknowledgments

The research described in this paper was financially supported by the National Natural Science Foundation of China (Grant No. 51504016) and Fundamental Research Funds for the Central Universities (Grant No. FRF-TP-18-016A3) and Technology top talent support project of Guizhou Provincial Education Department ([2017]098).

References

Agar, J.G., Morgenstern, N.R. and Scott, J.D. (1987), "Shear strength and stress-strain behavior of Athabasca oil sand at elevated temperatures and pressures", *Can. Geotech. J.*, **24**(1), 1-10. https://doi.org/10.1139/t87-001.

Alejano, L.R. and Alonso, E. (2005), "Considerations of the dilatancy angle in rocks and rock masses", *Int. J. Rock Mech. Min. Sci.*, **42**(4), 481-507. https://doi.org/10.1016/j.ijrmms.2005.01.003.

Alejano, L.R., Alfonso, R.D. and Veiga, M. (2012), "Plastic radii and longitudinal deformation profles of tunnels excavated in strain-softening rock masses", *Tunn. Undergr. Sp. Technol.*, **30**, 169-182. https://doi.org/10.1016/j.tust.2012.02.017.

Alonso, E., Alejano, L.R., Varas, F., Fdez-Manin, G. and Carranza-Torres, C. (2003), "Ground response curves for rock masses exhibiting strain-softening behaviour", *Int. J. Numer. Anal. Meth. Geomech.*, **27**(13), 1153-1185. https://doi.org/10.1002/nag.315.

Brown, E.T., Bray, J.W. and Santarelli, F.J. (1989), "Influence of stress-dependent elastic moduli on stresses and strains around axisymmetric boreholes", *Rock Mech. Rock Eng.*, **22**(3), 189-203. https://doi.org/10.1007/BF01470986.

Brown, E.T., Bray, J.W., Ladanyi, B. and Hoek, E. (1983), "Ground response curves for rock tunnels", *J. Geotech. Eng.*, **109**(1), 15-39. https://doi.org/10.1061/(ASCE)0733-9410(1983)109:1(15).

Carranza-Torres, C. and Fairhurst, C. (1999), "The elasto-plastic response of underground excavations in rock masses that satisfy the Hoek-Brown failure criterion", *Int. J. Rock Mech. Min. Sci.*, **36**(6), 777-809. https://doi.org/10.1016/S0148-9062(99)00047-9.

Carranza-Torres, C. and Fairhurst, C. (2000), "Application of the convergence-confnement method of tunnel design to rock masses that satisfy the hoek-brown failure criterion", *Tunn. Undergr. Sp. Technol.*, **15**(2), 187-213. https://doi.org/10.1016/S0886-7798(00)00046-8.

Chen, S.J., Yin, D.W., Jiang, N., Wang, F. and Zhao, Z.H. (2019), "Mechanical properties of oil shale-coal composite samples", *Int. J. Rock Mech. Min. Sci.*, **123**, 104120. https://doi.org/10.1016/j.ijrmms.2019.104120.

Cui, L., Sheng, Q., Zheng, J.J., Cui, Z., Wang, A. and Shen, Q. (2019), "Regression model for predicting tunnel strain in strain-softening rock mass for underground openings", *Int. J. Rock Mech. Min. Sci.*, **119**, 81-97. https://doi.org/10.1016/j.ijrmms.2019.04.014.

Cui, L., Zheng, J.J., Dong, Y.K., Zhang, B. and Wang, A. (2017), "Prediction of critical strains and critical support pressures for circular tunnel excavated in strain-softening rock mass", *Eng. Geol.*, **224**, 43-61. https://doi.org/10.1016/j.enggeo.2017.04.022.

Cui, L., Zheng, J.J., Zhang, R.J. and Dong, Y.K. (2015), "Elasto-plastic analysis of a circular opening in rock mass with confining stress-dependent strain-softening behaviour", *Tunn. Undergr. Sp. Technol.*, **50**, 94-108. https://doi.org/10.1016/j.tust.2015.07.001.

Detournay, E. (1986), "Elasto-plastic model of a deep tunnel for a rock with variable dilatancy", *Rock Mech. Rock Eng.*, **19**(2), 99-108. https://doi.org/10.1007/BF01042527.

Fahimifar, A., Ghadami, H. and Ahmadvand, M. (2015), "The ground response curve of underwater tunnels, excavated in a strain-softening rock mass", *Geomech. Eng.*, **8**(3), 323-359. https://doi.org/10.12989/gae.2015.8.3.323.

Feng, G., Kang, Y., Wang, X.C., Hu, Y.Q. and Li, X.H. (2020a), "Investigation on the failure characteristics and fracture classification of shale under brazilian test conditions", *Rock Mech. Rock Eng.*, **53**, 3325-3340. https://doi.org/10.1007/s00603-020-02110-6.

Feng, G., Wang, X.C., Wang, M. and Kang, Y. (2020b), "Experimental investigation of thermal cycling effect on fracture characteristics of granite in a geothermal-energy reservoir", *Eng. Fract. Mech.*, 107180. https://doi.org/10.1016/j.engfracmech.2020.107180.

Hoek, E. and Brown, E.T. (1997), "Practical estimates of rock mass strength", *Int. J. Rock Mech. Min. Sci. Geomech. Abstr.*, **34**, 1165-1186. https://doi.org/10.1016/S1365-1609(97)80069-X.

Hoek, E., Carranza-Torres, C. and Corkum, B. (2002), "Hoek-Brown failure criterion-2002 edition", *Proceedings of the 5th North American Rock Mechanics Symposium*, Toronto, Ontario, Canada.

Huang, H., Babadagli, T., Chen, X., Li, H.Z. and Zhang, Y.M. (2020), "Performance comparison of novel chemical agents for mitigating water-blocking problem in tight gas sandstones", *SPE. Reserv. Eval. Eng.*, 1-9. https://doi.org/10.2118/199282-PA.

Jiang, N., Wang, C.X., Pan, H.Y., Yin, D.W. and Ma, J.B. (2020), "Modeling study on the influence of the strip filling mining sequence on mining-induced failure", *Energy Sci. Eng.*, **8**(6), 2239-2255. https://doi.org/10.1002/ese3.660.

Kaliszky, S. (1989), *Plasticity: Theory and Engineering Applications*, Elsevier, Amsterdam, The Netherlands.

Kulhawy, F.H. (1975), "Stress deformation properties of rock and rock discontinuities", *Eng. Geol.*, **9**(4), 327-350. https://doi.org/10.1016/0013-7952(75)90014-9.

Lee, Y.K. and Pietruszczak, S. (2008), "A new numerical procedure for elasto-plastic analysis of a circular opening excavated in a strain-softening rock mass", *Tunn. Undergr. Sp. Technol.*, **23**(5), 588-599. https://doi.org/10.1016/j.tust.2007.11.002.

Li, Y., Cao, S., Fantuzzi, N. and Liu, Y. (2015), "Elasto-plastic analysis of a circular borehole in elastic-strain softening coal seams", *Int. J. Rock Mech. Min. Sci.*, **100**(80), 316-324. https://doi.org/10.1016/j.ijrmms.2015.10.002.

Nawrocki, P.A. and Dusseault, M.B. (1995), "Modelling of damaged zones around openings using radius-dependent Young's modulus", *Rock Mech. Rock Eng.*, **28**(4), 227-239. https://doi.org/10.1007/BF01020228.

Park, K.H., Tontavanich, B. and Lee, J.G. (2008), "A simple procedure for ground response curve of circular tunnel in elastic-strain softening rock masses", *Tunn. Undergr. Sp. Technol.*, **23**(2), 151-159. https://doi.org/10.1016/j.tust.2007.03.002.

Ren, D.Z., Zhou, D.S., Liu, D.K., Dong, F.J., Ma, S.W. and Huang, H. (2019), "Formation mechanism of the upper triassic Yanchang formation tight sandstone reservoir in Ordos basin—Take Chang 6 reservoir in Jiyuan oil field as an example", *J. Petrol. Sci. Eng.*, **178**, 497-505. https://doi.org/10.1016/j.petrol.2019.03.021.

Ren, F.Q., Zhu, C. and He, M.C. (2020), "Moment tensor analysis of acoustic emissions for cracking mechanisms during schist strain burst", *Rock Mech. Rock Eng.*, **53**(1), 153-170. https://doi.org/10.1007/s00603-019-01897-3.

Santarelli, F.J. (1987), "Theoretical and experimental investigation of the stability of the axisymmetric borehole", Ph.D. Dissertation, University of London, London, U.K.

Shan, P.F. and Lai, X.P. (2020), "An associated evaluation methodology of initial stress level of coal-rock masses in steeply inclined coal seams, Urumchi coal field, China", *Eng. Comput.*, **37**(6), 2177-2192. https://doi.org/10.1108/EC-07-2019-0325.

Sharan, S.K. (2008), "Analytical solutions for stresses and displacements around a circular opening in a generalized Hoek-brown rock", *Int. J. Rock Mech. Min. Sci.*, **45**(1), 78-85. https://doi.org/10.1016/j.ijrmms.2007.03.002.

Shi, G.C., Yang, X.J., Yu, H.C. and Zhu, C. (2018), "Acoustic emission characteristics of creep fracture evolution in doublefracture fine sandstone under uniaxial compression", *Eng. Fract. Mech.*, **210**, 13-28. https://doi.org/10.1016/j.engfracmech.2018.09.004.

Tao, Z.G., Wang, Y., Zhu, C., Xu, H.X., Li, G. and He, M.C. (2019), "Mechanical evolution of constant resistance and large deformation anchor cables and their application in landslide monitoring", *B. Eng. Geol. Environ.*, **78**, 4787-4803. https://doi.org/10.1007/s10064-018-01446-2.

Timoshenko, S.P. and Goodier, J.N. (1982), *Theory of Elasticity*, McGraw-Hill Book Co.

Walton, G., Hedayat, A. and Rahjoo, M. (2019), "Relating plastic potential function to experimentally obtained dilatancy observations for geomaterials with a confinement-dependent dilation angle", *Int. J. Geomech.*, **19**(8). https://doi.org/10.1061/(ASCE)GM.1943-5622.0001484.

Wang, C.X., Shen, B.T., Chen, J.T., Tong, W.X., Jiang, Z., Liu, Y. and Li, Y.Y. (2020b), "Compression characteristics of filling gangue and simulation of mining with gangue backfilling: An experimental investigation", *Geomech. Eng.*, **20**(6), 485-495. https://doi.org/10.12989/gae.2020.20.6.485.

Wang, F.Y. and Qian, D.L. (2018), "Difference solution for a circular tunnel excavated in strain-softening rock mass considering decayed confinement", *Tunn. Undergr. Sp. Technol.*, **82**, 66-81. https://doi.org/10.1016/j.tust.2018.08.001.

Wang, J., Ning, J.G., Qiu, P.Q., Yang, S. and Shang, H.F. (2019), "Microseismic monitoring and its precursory parameter of hard roof collapse in longwall faces: A case study", *Geomech. Eng.*, **17**(4), 375-383. https://doi.org/10.12989/gae.2019.17.4.375.

Wang, X., Yuan, W., Yan, Y.T. and Zhang, X. (2020a), "Scale effect of mechanical properties of jointed rock mass: A numerical study based on particle flow code", *Geomech. Eng.*, **21**(3), 259-268. https://doi.org/10.12989/gae.2020.21.3.259.

Yin, Q., Ma, G.W., Jing, H.W., Wang, H.D., Su, H.J., Wang, Y.C. and Liu, R.C. (2017), "Hydraulic properties of 3D rough-walled fractures during shearing: An experimental study", *J. Hydrol.*, **555**, 169-184. https://doi.org/10.1016/j.jhydrol.2017.10.019.

You, M.Q. (2003), "Effect of confining pressure on the Young's modulus of rock specimen and the friction in fissures", *Rock Soil Mech.*, **S2**, 167-170. https://doi.org/10.16285/j.rsm.2003.s2.038.

Yuan, S.C. and Harrison, J. (2004), "An empirical dilatancy index for the dilatant deformation of rock", *Int. J. Rock Mech. Min. Sci.*, **41**(4), 679-686. https://doi.org/10.1016/j.ijrmms.2003.11.001.

Zhang, C.G., Zhao, J.H., Zhang, Q.H. and Hu, X.D. (2012a), "A new closed-form solution for circular openings modeled by the unified strength theory and radius-dependent Young's modulus", *Comput. Geotech.*, **42**, 118-128. https://doi.org/10.1016/j.compgeo.2012.01.005.

Zhang, N., Liu, W., Zhang, Y., Shan, P.F. and Shi, X.L. (2020a), "Microscopic pore structure of surrounding rock for underground strategic petroleum reserve (SPR) caverns in bedded rock salt", *Energies*, **13**(7), 1565. https://doi.org/10.3390/en13071565.

Zhang, Q., Jiang, B.S., Wu, X.S., Zhang, H.Q. and Han, L.J. (2012b), "Elasto-plastic coupling analysis of circular openings in elasto-brittle-plastic rock mass", *Theor. Appl. Fract. Mech.*, **60**(1), 60-67. https://doi.org/10.1016/j.tafmec.2012.06.008.

Zhang, Q., Zhang, C.H., Jiang, B.S., Li, N. and Wang, Y.C. (2018), "Elastoplastic coupling solution of circular openings in strain-softening rock mass considering pressure-dependent effect", *Int. J. Geomech.*, **18**(1), 04017132. https://doi.org/10.1061/(ASCE)GM.1943-5622.0001043.

Zhang, Y., Cao, S.G., Zhang, N. and Zhao, C.Z. (2020b), "The application of short-wall block backfill mining to preserve surface water resources in northwest China", *J. Cleaner Prod.*, **261**, 121232. https://doi.org/10.1016/j.jclepro.2020.121232.

Zhao, X.G. and Cai, M. (2010a), "A mobilized dilation angle model for rocks", *Int. J. Rock Mech. Min. Sci.*, **47**(3), 368-384. https://doi.org/10.1016/j. ijrmms.2009.12.007.

Zhao, X.G. and Cai, M. (2010b), "Influence of plastic shear strain and confinement-dependent rock dilation on rock failure and displacement near an excavation boundary", *Int. J. Rock Mech. Min. Sci.*, **47**(5), 723-738. https://doi.org/10.1016/j.ijrmms.2010.04.003.

Zou, J.F., Yang, T., Ling, W., Guo, W.J. and Huang, F.L. (2019), "A numerical stepwise approach for cavity expansion problem in strain-softening rock or soil mass", *Geomech. Eng.*, **18**(3), 225-234. https://doi.org/10.12989/gae.2019.18.3.225.

CC